

Article

Merelaniite, $\text{Mo}_4\text{Pb}_4\text{VSbS}_{15}$, a New Molybdenum-Essential Member of the Cylindrite Group, from the Merelani Tanzanite Deposit, Lelatema Mountains, Manyara Region, Tanzania

John A. Jaszczak^{1,*}, Michael S. Rumsey², Luca Bindi³, Stephen A. Hackney⁴, Michael A. Wise⁵, Chris J. Stanley² and John Spratt⁶

¹ Department of Physics and the A. E. Seaman Mineral Museum, Michigan Technological University, 1400 Townsend Dr., Houghton, MI 49931-1295, USA

² Department of Earth Sciences, Natural History Museum, Cromwell Road, London SW7 5BD, UK; m.rumsey@nhm.ac.uk (M.S.R.); c.stanley@nhm.ac.uk (C.J.S.)

³ Dipartimento di Scienze della Terra, Università di Firenze, Via La Pira 4, I-50121 Firenze, Italy; luca.bindi@unifi.it

⁴ Department of Materials Science and Engineering, Michigan Technological University, 1400 Townsend Dr., Houghton, MI 49931-1295, USA; hackney@mtu.edu

⁵ Department of Mineral Sciences, National Museum of Natural History, Smithsonian Institution, Washington, DC 20560, USA; wisem@si.edu

⁶ Department of Core Research Laboratories, Natural History Museum, Cromwell Road, London SW7 5BD, UK; j.spratt@nhm.ac.uk

* Correspondence: jaszczak@mtu.edu; Tel.: +1-906-487-2255

Academic Editor: Thomas N. Kerestedjian

Received: 7 September 2016; Accepted: 20 October 2016; Published: 28 October 2016

Abstract: Merelaniite is a new mineral from the tanzanite gem mines near Merelani, Lelatema Mountains, Simanjiro District, Manyara Region, Tanzania. It occurs sporadically as metallic dark gray cylindrical whiskers that are typically tens of micrometers in diameter and up to a millimeter long, although a few whiskers up to 12 mm long have been observed. The most commonly associated minerals include zoisite (variety tanzanite), prehnite, stilbite, chabazite, tremolite, diopside, quartz, calcite, graphite, alabandite, and wurtzite. In reflected polarized light, polished sections of merelaniite are gray to white in color, show strong bireflectance and strong anisotropism with pale blue and orange-brown rotation tints. Electron microprobe analysis ($n = 13$), based on 15 anions per formula unit, gives the formula $\text{Mo}_{4.33}\text{Pb}_{4.00}\text{As}_{0.10}\text{V}_{0.86}\text{Sb}_{0.43}\text{Bi}_{0.33}\text{Mn}_{0.05}\text{W}_{0.05}\text{Cu}_{0.03}(\text{S}_{14.70}\text{Se}_{0.30})_{\Sigma 15}$, ideally $\text{Mo}_4\text{Pb}_4\text{VSbS}_{15}$. An arsenic-rich variety has also been documented. X-ray diffraction, electron diffraction, and high-resolution transmission electron microscopy show that merelaniite is a member of the cylindrite group, with alternating centered pseudo-tetragonal (Q) and pseudo-hexagonal (H) layers with respective PbS and MoS_2 structure types. The Q and H layers are both triclinic with space group $C1$ or $C\bar{1}$. The unit cell parameters for the Q layer are: $a = 5.929(8) \text{ \AA}$; $b = 5.961(5) \text{ \AA}$; $c = 12.03(1) \text{ \AA}$; $\alpha = 91.33(9)^\circ$; $\beta = 90.88(5)^\circ$; $\gamma = 91.79(4)^\circ$; $V = 425(2) \text{ \AA}^3$; and $Z = 4$. For the H layer, $a = 5.547(9) \text{ \AA}$; $b = 3.156(4) \text{ \AA}$; $c = 11.91(1) \text{ \AA}$; $\alpha = 89.52(9)^\circ$; $\beta = 92.13(5)^\circ$; $\gamma = 90.18(4)^\circ$; $V = 208(2) \text{ \AA}^3$; and $Z = 2$. Among naturally occurring minerals of the cylindrite homologous series, merelaniite represents the first Mo-essential member and the first case of triangular-prismatic coordination in the H layers. The strongest X-ray powder diffraction lines [d in \AA (I/I_0)] are 6.14 (30); 5.94 (60); 2.968 (25); 2.965 (100); 2.272 (40); 1.829 (30). The new mineral has been approved by the IMA CNMNC (2016-042) and is named after the locality of its discovery in honor of the local miners.

Keywords: merelaniite; cylindrite group; molybdenum; lead; Merelani tanzanite deposit; Tanzania

1. Introduction

Merelaniite, from Merelani, Tanzania, was first identified unknowingly in 2012 by Simonoff and Wise as thin wires of “molybdenite” piercing chabazite crystals [1–3]. Subsequent Raman spectroscopy and energy-dispersive X-ray spectrometry by one of the authors (JAJ) indicated that the phase was likely a new mineral. It is plausible that it is the same or very similar to the phase noted by Zakrzewski et al. in 1982 as an “unnamed Pb-Mo sulfide” from the Sätra mine in Sweden [4], since listed by Smith and Nickel [5] as valid unknown “UM1982-13-S:MoPb”, and perhaps also valid unknown “UM1971-18-S:MoPbSb” from Kayrakty, Kazakhstan [6].

During the years 2011–2014, spurred by the discovery of a very large wurtzite crystal (now in the Natural History Museum, London BM 2012,220; [7]) and the subsequent identification of extremely large alabandite crystals from the same mineralogical assemblage, two of the authors (JAJ and MSR) started performing systematic analyses of the sulfides available on the mineral market from the graphite and tanzanite producing mines of the Merelani region in Tanzania. This review culminated in the publication of a collector-based overview in *The Mineralogical Record* [7], and the identification of several exotic and/or unusually well crystallized sulfide phases. In amongst these phases the authors noted the presence of what they termed ‘incompletely characterized sulfide whiskers’. These “whiskers” were described as tightly coiled metallic cylinders with a chemical composition predominant in molybdenum, lead, and sulfur. They were found alongside many different mineral species from the assemblage, yet at the time, they defied a simple explanation. It is this phase that is herewith described as the new mineral merelaniite, which is identified as the first naturally occurring molybdenum-essential member of the cylindrite group of minerals. The new mineral has been approved by the Commission of New Minerals, Nomenclature and Classification (CNMNC) of the IMA (2016-042) and is named after the township of Mererani, known more commonly in the mineral and gemological communities as “Merelani”, in honor of the local miners, past and present, living and working in the region. Samples from the holotype specimen, all of which were extracted from crevices on a single unusually large (11 cm) alabandite crystal from Simon Harrison (initially assigned numbers 3665 and 3666), have been deposited in the collections of the Natural History Museum (London), the A. E. Seaman Mineral Museum, the Smithsonian Institution’s National Museum of Natural History (cataloged under NMNH 177015), and one of the authors (JAJ) under numbers 3665 and 3666). Those in the Natural History Museum (London) are cataloged under BM 2016,100, and include polished grains embedded in a microprobe block, as well as isolated fragments of whiskers used for the crystallographic, chemical and optical studies. Those in the A. E. Seaman Mineral Museum (cataloged under DM 31323, DM 31324, and DM 31325) include polished sections embedded in epoxy mounts used for optical studies, as well as a small cluster of whiskers with graphite. The crystals used for the X-ray crystallographic investigations are kept at the Department of Earth Sciences, University of Firenze, Italy. Initial Raman and chemical studies were performed on a specimen in the collection of the Smithsonian Institution (temporary research number 3323, and now also cataloged under NMNH 177015).

2. Occurrence and Geological Setting

The new mineral merelaniite (Figures 1–3) occurs rarely and sporadically on specimens extracted from the gem mines in the Merelani hills near the town of Arusha, Lelatema Mountains, Manyara Region, Tanzania (approximated by 3°35′0 S, 37°0′30 E). Unfortunately, due to the nature of the opportunistic artisanal mining across this region for the tanzanite variety of zoisite, the tsavorite variety of grossular, and more recently the rare sulfides, the exact geological location of any specimen known to contain merelaniite is undocumented and unknown. All the specimens so far identified that contain merelaniite have been obtained through the secondary mineral markets. The specimens were originally sold for other more obvious and desirable minerals, and were unaccompanied by any further detailed locality information. It may be noteworthy in tracking down an exact locality that most merelaniite specimens have been identified since the assumed sulfide-rich “zone” that produced the

wurtzite and alabandite crystals that became available to collectors (around 2011–2013). Merelaniite has likely not been recorded in situ due to its rarity, small size, and cursory visual similarity to graphite, which is ubiquitous in the region.

The relevant regional geology of the Merelani region is dominated by ultrahigh temperature (granulite facies) metamorphism of organic rich sedimentary “black shale” deposits rich in vanadium [8–10]. Four phases of deformation have been identified in one study [8] with temperatures in the first phase estimated as high as 1000 °C with pressures up to 10–12 Kbar. The formation mechanism of the large sulfide crystals has not been extensively studied to date, but association with ubiquitous well-crystallized “flake” graphite would hint at high temperatures and stable crystallizing conditions being relevant. The partial coating of the sulfides and later infilling of cracks and voids by lower-grade metamorphic phases such as the zeolites and prehnite indicates these multiple phases of reworking and deformation may be particularly relevant to the growth of merelaniite, potentially placing it between the highest initial deformation and one or more of the retrograde events. It is beyond the scope of this new-mineral description to determine a conclusive paragenetic model or to describe the geology of the Merelani hills in more detail; for the latter, references [9,11] are recommended.

Although merelaniite is clearly rare, given the amount of prehnite, diopside, wurtzite, and alabandite material on the market at the moment, the authors suspect that many other specimens ($c.10^2$) containing trace amounts of merelaniite already exist extracted from the mines. Merelaniite has been recorded so far in association with, calcite, chabazite, diopside, graphite, quartz, fluorapatite, prehnite, stilbite, tremolite, laumontite, titanite, zoisite (tanzanite), alabandite, clausthalite, pyrite, and wurtzite (Figures 1–3). Simple paragenetic associations distinguish merelaniite as forming after alabandite-wurtzite, yet prior to quartz, calcite, prehnite, fluorapatite, zoisite, and zeolites, which have all been observed to fully or partially encapsulate fully-formed merelaniite whiskers (Figures 1–3 show many but not all of these associations). The merelaniite whiskers on the holotype specimen were found in crevices loosely attached to the surfaces of large alabandite crystals, intimately associated with masses of loosely aggregated yet well-formed graphite crystals (Figure 4).



Figure 1. Optical photographs of merelaniite and some associated minerals: (a) 0.73-mm-long “cylindrical” whisker of merelaniite associated with tremolite, prehnite, and chabazite (private collection); (b) Whisker of merelaniite (0.9-mm section), associated with calcite, showing undulating diameters (Simon Harrison collection; sample 3941); (c) 2.5-mm section of a 5-mm-long merelaniite whisker (maximum diameter 0.18 mm) showing naturally unraveled ribbons, some partially enclosed in calcite, and associated with yellow prehnite (Simon Harrison collection; sample 3941).

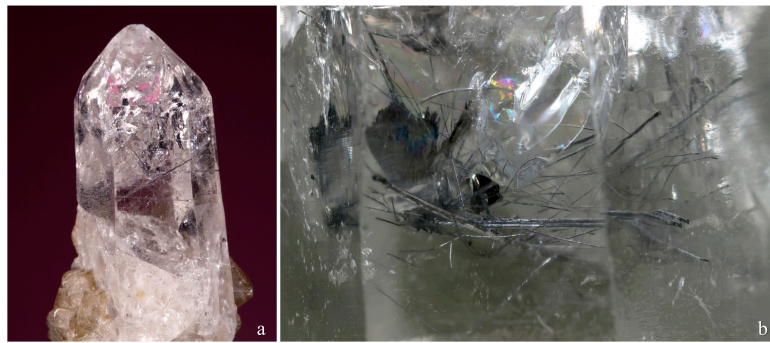


Figure 2. Optical photographs of (a) 2.8-cm-tall quartz crystal with inclusions of merelaniite whiskers, also associated with chabazite crystals; (b) close-up of (a) showing merelaniite, graphite and an unidentified fan-shaped phase at the left of the image (~8 mm wide field-of-view). (A. E. Seaman Mineral Museum collection DM 31315; ex. Simon Harrison collection.).



Figure 3. Optical photograph of whiskers of merelaniite to 2.8 mm long associated with crystals of stilbite and graphite (sample 3665c), found in a small crevice on an 11-cm long alabandite crystal (private collection).

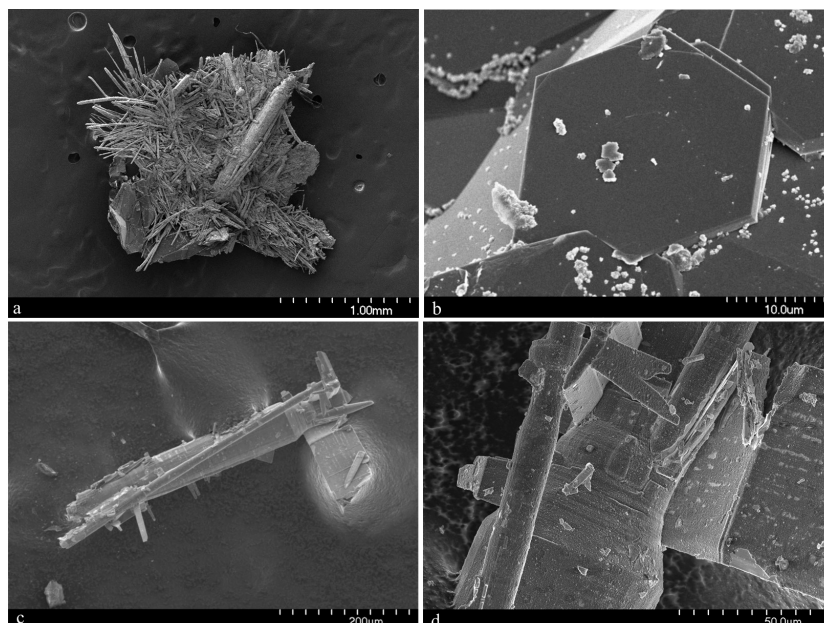


Figure 4. *Cont.*

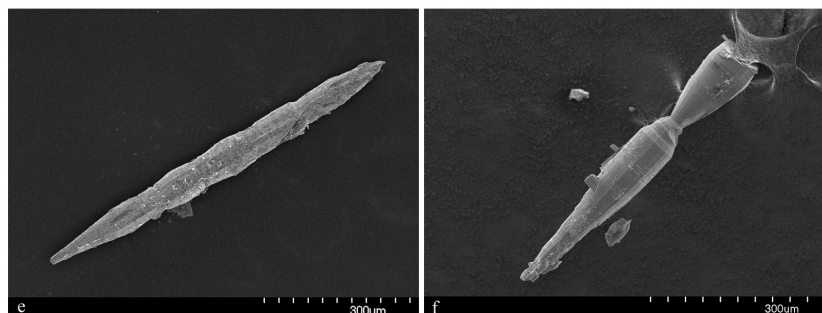


Figure 4. Scanning electron microscope (SEM) images of samples taken from the holotype specimen. (a) Cluster of merelaniite whiskers with one notably larger cylinder, associated with graphite. (Sample 3666i-190i.); (b) Section of a merelaniite-graphite cluster showing well-formed graphite crystals (Sample 3666i-190h.); (c,d) Merelaniite whiskers showing partially un-wound layers. (Sample 3666-196a.); (e,f) Individual whiskers showing conical ends and undulating diameters (Samples 3666i 190d and 3666 196c). Images taken using a Hitachi S-4700 field-emission SEM (Hitachi, Tokyo, Japan).

3. Detailed Description

3.1. Appearance and Physical Properties

Merelaniite occurs individually and in clusters as dark gray metallic whiskers of circular cross-section (Figures 1–5). On further inspection, especially by scanning electron microscopy, the whiskers are revealed to be composed of tightly coiled layers and are perhaps better described as “scrolls” (Figure 5c,d), although this is not often visible under optical microscopy. It is similar in its appearance to other minerals of the cylindrite-type.

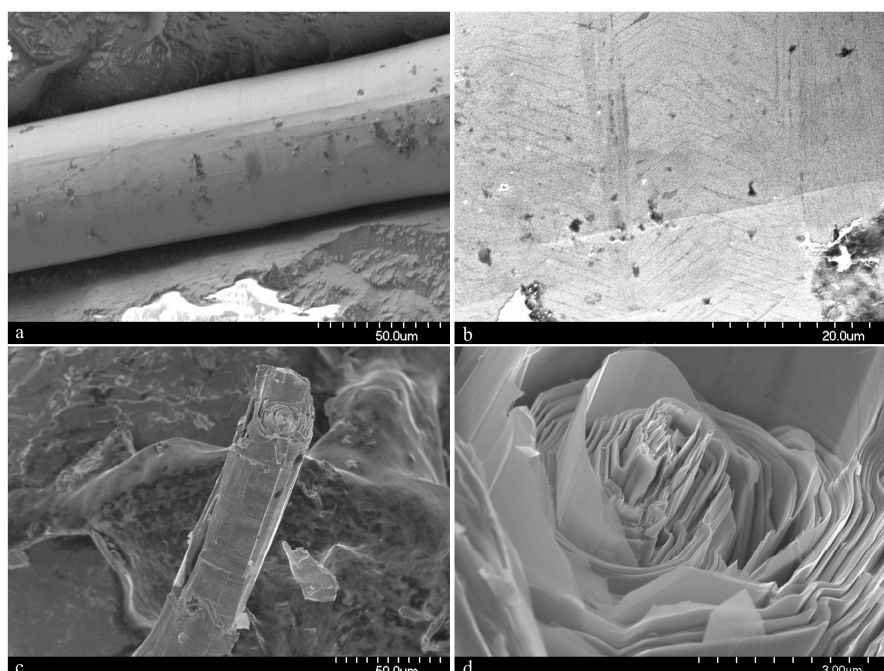


Figure 5. SEM (Hitachi S-4700) images of merelaniite (Smithsonian Institution specimen NMNH 177015, reference 3323). (a) Merelaniite cylinder partially exposed from enclosing calcite; (b) Close-up image of the surface showing visible growth-layer steps; (c,d) The same merelaniite whisker after being broken, showing the curved lamellar (scroll) structure.

The whiskers commonly have a varying diameter along their length (Figure 1b,c and Figure 4c–f), and in some examples parts of the individual lamella can be observed “peeling” away from the main cylinder or scroll (Figures 1c and 4c,d), a process which may in part lead to the undulations observed. The whiskers regularly terminate in a conical shape (Figures 1a and 4e,f). When viewed end on under scanning electron microscopy, broken whiskers reveal the lamellar nature of the scroll-like structure (Figure 5c,d). As a member of the extended cylindrite group of minerals, traditional crystals are not observed. Instead the scroll-like whiskers are the manifestation of a single tightly coiled flat crystal.

In the holotype specimen, the richest known example found to date, some whiskers were a little over 10 mm in length, with 12 mm being the longest individual recorded so far. The thickness, however, is never more than 100 μm . More regularly the whiskers are no more than a millimeter in length and just tens of microns in width.

Although merelaniite has been found on a number of different specimens, most of the whiskers studied during this investigation and all of those designated as “part of holotype” were isolated from just one specimen, an extremely large alabandite crystal (11 cm in maximum dimension), that contained a crevice filled with a chaotic mass of loosely bound merelaniite whiskers inter-grown with equally loosely aggregated graphite crystals (see reference [7] (Figure 5d,g, pp. 42–25), and reference [10] (p. 43)), along with some rounded brown titanite crystals and colorless diopside crystals (the graphite, titanite and diopside crystals all range in size from one to a few hundred micrometers across). It is our understanding that this specimen is now in private hands; however, before it was purchased a volume of whiskers from the main crevice and a smaller crevice were removed for study by JAJ with permission of its then owner, Simon Harrison. Samples were subsequently passed to MSR and LB for further study. The whiskers removed from this sample (initially numbered 3665 and 3666) and used during the characterization of the material are deposited within several institutional mineral collections as noted in the Introduction.

The physical characteristics of merelaniite are summarized as follows:

- Habit: massive
- Forms: needles—cylindrical whiskers (tightly packed scrolls)
- Twinning: None observed
- Color: dark-gray, metallic
- Streak: dark-gray to black
- Luster: metallic; opaque
- Fluorescence: not fluorescent in SW or LW UV light
- Hardness (Mohs): impossible to determine accurately due to size and scroll-like lamellar nature of the material
- Tenacity: malleable, flexible
- Cleavage: perfect on {001}
- Fracture: splintery
- Density (meas.): not determined due to paucity of material
- Density (calc.) = $4.895 \text{ g}\cdot\text{cm}^{-3}$ (from ideal formula, unit-cell volumes of the two pseudo-layers and $Z = 1$)

3.2. Optical Properties

In reflected polarized light, polished sections of merelaniite show the following:

- Color: grayish-white
- Internal reflections: none
- Pleochroism: weak
- Bireflectance: strong. Pale gray (axial sections) to almost white (longitudinal sections) (Figure 6a,b and Figure 7a,b)

- Anisotropism: strong in generally neutral rotation tints. Polished samples showed blue and pale orange-brown tints in slightly uncrossed polarizers (Figure 6c,d and Figure 7c).

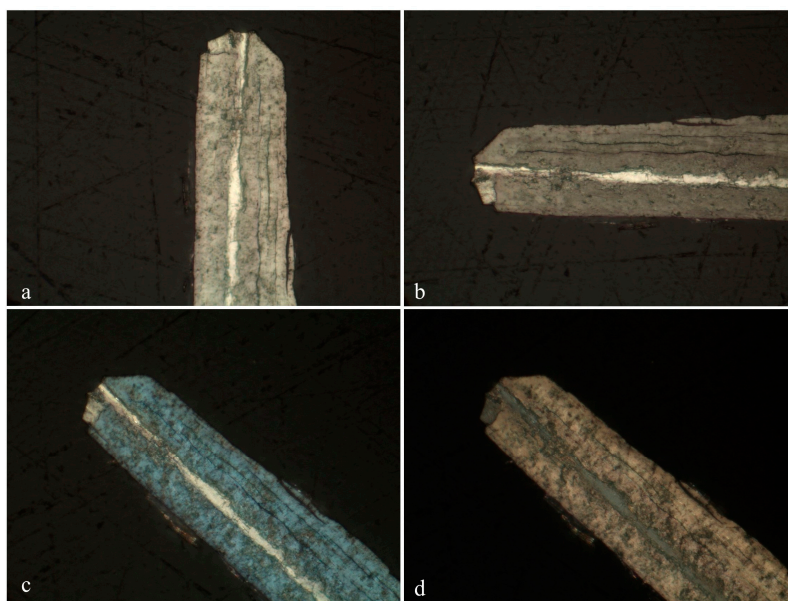


Figure 6. Reflected light microscope images of longitudinal sections of a polished merelaniite whisker (0.06 mm diameter) (Nikon Optiphot-Pol petrographic microscope): (a) Polarizer and analyzer both aligned vertically, parallel to the whisker axis; (b) Polarizer and analyzer both aligned vertically, perpendicular to the whisker axis; (c,d) Analyzer aligned vertically and polarizer slightly plus/minus un-crossed. It is not certain if the core of the whisker reflects more brightly due to a possible chemical difference between the core and outer region or is simply because the layers in the core are parallel to the polished surface. (A. E. Seaman Mineral Museum collection DM 31324, reference 3666ax2).

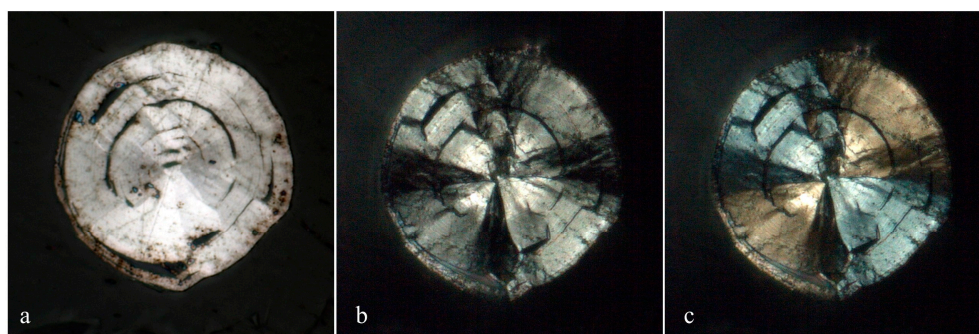


Figure 7. Reflected light microscope images of a polished axial section of a merelaniite whisker (0.09 mm diameter) (Nikon Optiphot-Pol petrographic microscope): (a) polarizer and analyzer both aligned horizontally; (b) crossed polarizers; and (c) slightly un-crossed polarizers. (A. E. Seaman Mineral Museum collection DM 31323, reference 3666cr2).

Reflectance measurements of merelaniite, using a WTiC standard in air were performed using ONYX software on a Zeiss Axiotron microscope (Carl Zeiss AG, Oberkochen, Germany) in conjunction with a J & M TIDAS diode-array spectrophotometer (J & M Analytik AG, Essingen, Germany). Merelaniite shows greatest reflectance and bireflectance toward the blue end of the spectrum. Tabulated data along with interpolated COM (Commission on Ore Mineralogy) values (highlighted) are presented in Table 1. The interpolated reflectance percentages (R_1 and R_2 , respectively) at the four COM wavelengths are 36.8, 46.3 (470 nm); 35.6, 44.1 (546 nm); 34.8, 42.3 (589 nm); and 34.3, 39.9 (650 nm).

Table 1. Reflectance measurements of merelaniite using a WTiC standard taken in air. Measurements of R_1 and were taken on an axial cross-section, and R_2 measurements were taken on a longitudinal section. Interpolated COM (Commission on Ore Mineralogy) values are highlighted in boldface italics font.

λ nm	R_1	R_2
400	37.6	47.6
420	37.4	47.2
440	37.2	46.8
460	36.9	46.5
470	36.8	46.3
480	36.6	46.1
500	36.3	45.7
520	36.0	45.1
540	35.7	44.4
546	35.6	44.1
560	35.4	43.5
580	35.0	42.7
589	34.8	42.3
600	34.6	41.8
620	34.4	41.0
640	34.3	40.2
650	34.3	39.9
660	34.2	39.6
680	34.1	39.2
700	34.0	39.0

3.3. Raman Spectroscopy

Raman spectroscopy was performed on a curved surface of a cylindrical whisker freshly exposed from enclosing calcite (piece of sample 3323) using dilute acetic acid, and on the polished sections of the samples shown in Figures 6 and 7. The spectra shown in Figure 8 were collected at Miami University (Oxford, OH, USA) using a Renishaw inVia Raman spectrometer (Renishaw plc, Wotton-under-Edge, Gloucestershire, UK) in backscattering geometry, with unpolarized incident laser radiation at 633-nm and 785-nm wavelengths, respective diffraction gratings with 1800 lines/mm and 1200 lines/mm, a 50 \times objective lens, and a laser spot size of approximately 2 μ m. A neutral density filter was used to reduce the power of the laser at the sample to less than 3 mW to avoid sample heating effects (peak shifts and broadening) and sample damage. Laser-induced damage was observed at higher power levels that led to the occurrence of intense but spurious bands at 319, 870, and 930 cm^{-1} .

Although the relative intensities vary to some degree with respect to sample and excitation wavelength, all of the spectra show prominent Raman peaks at 324, 379, 390, and 401 cm^{-1} , with the peak at 401 cm^{-1} typically being the most intense. A less prominent peak is also observed in most spectra near 350 cm^{-1} . An intense broad band manifests between 133 and 245 cm^{-1} , while less intense broad bands are centered near approximately 450, 570, and 780 cm^{-1} . The broad band at 570 cm^{-1} appears to be two bands centered at 568 and 621 cm^{-1} when using 785-nm radiation. Raman shifts greater than 900 cm^{-1} were not observed in any spectra except for several reproducible bands at 916, 1176, 1374, and 1619 cm^{-1} that can be seen in the spectrum of a polished whisker (3666ax2) excited with 633-nm radiation midway between the whisker axis and the surface. These peaks did not manifest from this sample using 785-nm radiation. Preliminary spectra were taken at Michigan Technological University with a LabRAM HR800 Raman spectrometer (HORIBA Jobin Yvon, Edison, NJ, USA) in backscattering geometry using polarized 633-nm radiation. These showed only slight changes in the relative peak intensities upon rotation of the whisker axis from parallel to perpendicular relative to the incident direction of polarization of the laser. Note that the spectrum from the brightly reflecting region near the whisker axis (3666ax2 core) is virtually indistinguishable from the spectrum from the natural surface of whisker 3323. A comparative search of Raman spectra of minerals in the RRUFF database using the CrystalSleuth program [12] yielded no satisfactory matches.

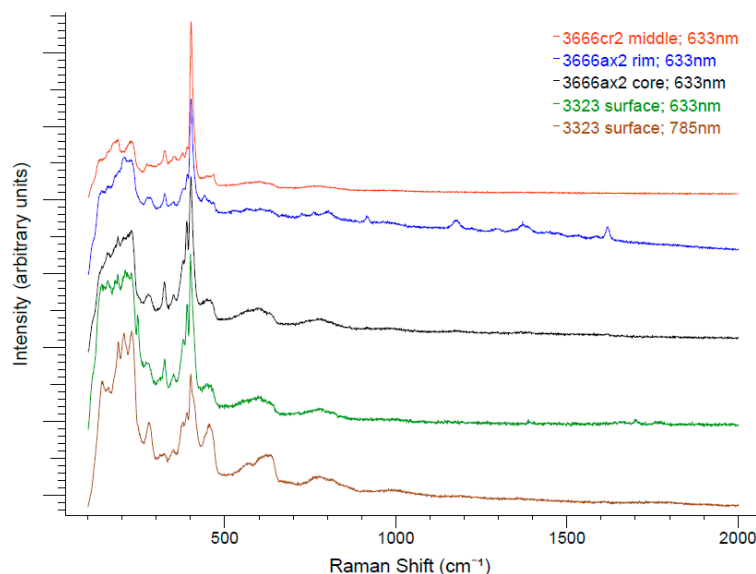


Figure 8. Representative Raman spectra, independently scaled and vertically shifted for clarity, from the surface of sample 3323, and from polished samples 3666ax2 and 3666cr2 using 633-nm and 785-nm incident radiation. The “3666cr2 middle” spectrum was taken from a region of the cross section shown in Figure 7 midway between the center and the surface. Spectra “3666ax2 rim” and “3666ax2 core” were taken from the longitudinal section of the whisker shown in Figure 6 from regions between the axis and the surface (rim), and from the brightly reflecting core, respectively.

In backscattering geometry, bulk MoS₂ exhibits three Raman peaks at approximately 33.5, 383.6 and 408.7 cm⁻¹, corresponding to E_{2g}² (interlayer shear), E_{2g}¹ (in-plane), and A_{1g} (out-of-plane) vibrational modes, respectively [13]. The E_{2g}¹ and A_{1g} peaks systematically broaden and shift to approximately 386 (E_{2g}¹) and 403 cm⁻¹ (A_{1g}), as the number of MoS₂ layers decreases from bulk to few-layers and ultimately to monolayer thickness. MoS₂ also exhibits several other strong first-order and second-order Raman peaks due to resonant Raman scattering when incident laser wavelengths 633 and 594 nm are employed [13,14]. On the other hand, while the high symmetry of bulk PbS precludes first-order Raman scattering, polycrystalline PbS thin films and PbS nanocrystals exhibit a broad band at 206 cm⁻¹, and overlapping broad bands at 410 and 462 cm⁻¹ [15]. Although merelaniite’s Raman spectra have some qualitative resemblance to the first-order Raman spectra of MoS₂ and other dichalcogenides, further studies of polarized Raman scattering using different excitation laser wavelengths will be necessary in order to more fully characterize its Raman spectrum.

3.4. Chemical Data

Several merelaniite whiskers ($n = 5$) from the loose pieces of BM 2016,100 were mounted onto a low-adhesive substrate, carefully placing the whiskers so as to mount them in a variety of perpendicular, inclined, and parallel orientations relative to the long axis of the whisker. They were then set in epoxy resin and polished using aluminum oxide abrasives to produce a flat surface (Probe Block P19396 of specimen BM 2016,100). Several of the perpendicular and parallel whiskers set successfully. Of those, two (one parallel and one perpendicular to the polished surface) were selected for electron microprobe analysis based on their superior homogeneity. Electron backscatter imaging showed clearly that other whiskers had increased chemical heterogeneity compared with the two selected and were therefore less suitable for chemical analysis. The two fragments studied were each about 50 μm in diameter, and the one set parallel was several hundred μm in length. Transects across each sample were performed using a CAMECA SX100 Microprobe (CAMECA, Gennevilliers, France) in WDS mode at the Natural History Museum in London using an accelerating voltage

of 20 kV, a beam current of 20 nA, and a spot size of 1 μm . Full spectrometer scans were performed beforehand in order to ascertain exactly which elements were present within the sample. The elements, S (ZnS), V [$\text{Pb}_5(\text{VO}_4)_3\text{Cl}$], Mn (MnTiO_3), Fe (Fe-metal), As (GaAs), Mo (Mo-metal), Sb (Sb-metal), W (W-metal), Pb (PbSe), Se (PbSe), Bi and Te (Bi_2Te_3), and Cu (Cu-metal) were sought and calibrated against appropriate standards (shown in parentheses). Obvious candidates, Ge and Zn, based on associated mineralogy present were sought for but found to be entirely lacking across all five samples. Te and Fe were observed in some samples, but not those ultimately chosen for the characterization of merelaniite.

A total of 41 spot analyses were performed over the two whiskers; 20 on the whisker in perpendicular orientation (Figure 9) and 21 on the whisker aligned in a parallel orientation. All 20 analyses on the perpendicular sample could be seen to correspond to the same phase but showed minor variations in total that are likely due to the analysis of micro-voids and epoxy which can be seen to exist between the scroll-like layers on the sample image (Figure 9). Only totals over 95% (by weight) were used to determine average quantitative data and those between 90%–95% were used to spot chemical trends. Totals under 90% were not included in the analysis. The whisker aligned parallel shows a bimodal composition, the “core” of which is the same as the 20 analyses from the perpendicular specimen. Combining all the analyses with totals above 95% resulted in 13 being used for the determination of an “average” empirical formula. It should be noted that using all 25 results that were above 90% produces an almost identical stoichiometry. Analyses from the 13 best data points are presented in Table 2, where corrections were applied for overlaps of Te/Sb, Bi/Pb, Bi/As, Sb/Bi, Sb/As, Sb/Mo, Pb/Mo, Pb/Bi, As/Bi, Mo/S, Mo/Pb, and Mo/Bi.

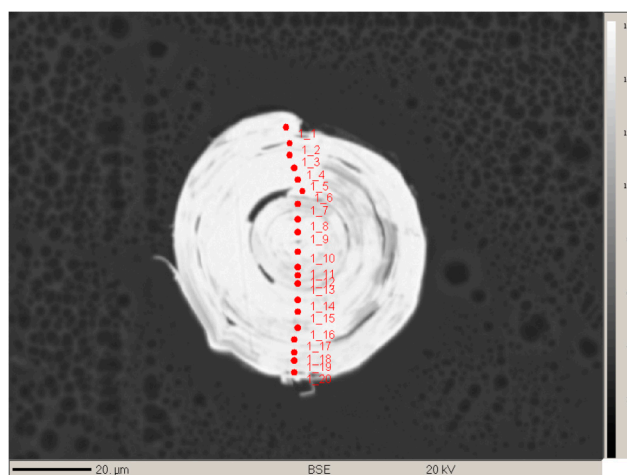


Figure 9. Polished axial section of a merelaniite “whisker” used for chemical analysis. The red spots indicate the areas analyzed across the transect. Note the scroll-like form and the clear voids between the individual layers which are attributed to have led to the weight% totals being a little under 100%. Sample BM 2016,100; probe block P19396.

The empirical formula calculated on the basis of 15 anions per formula unit is $\text{Mo}_{4.33}\text{Pb}_{4.00}\text{As}_{0.10}\text{V}_{0.86}\text{Sb}_{0.43}\text{Bi}_{0.33}\text{Mn}_{0.05}\text{W}_{0.05}\text{Cu}_{0.03}(\text{S}_{14.70}\text{Se}_{0.30})_{\Sigma 15}$. The simplified formula is $\text{Mo}_4\text{Pb}_4\text{VSbS}_{15}$, with a metal:sulfide (M:S) ratio of 2:3.

Table 2. Chemical data (wt %) for merelaniite.

Constituent	Mean wt %	Range	SD	Standards
S	24.05	23.60–24.42	0.25	ZnS
V	2.26	2.16–2.41	0.09	Pb ₅ (VO ₄) ₃ Cl
Mn	0.05	0.00–0.23	0.08	MnTiO ₃
As	0.39	0.23–0.87	0.16	GaAs
Mo	21.10	20.05–22.48	0.67	Mo
Sb	2.59	2.44–2.80	0.11	Sb
W	0.55	0.39–0.62	0.06	W
Pb	42.40	40.00–44.41	1.37	PbSe
Se	1.25	1.09–1.56	0.12	PbSe
Bi	3.56	3.05–4.12	0.33	Bi ₂ Te ₃
Cu	0.01	0.00–0.05	0.02	Cu
Total	98.20	95.94–100.54	1.62	N/A

3.5. Crystallography

Single-crystal X-ray studies were carried out at the CRIST centre of the University of Florence, Italy, using an Oxford Diffraction Xcalibur diffractometer (Oxford Diffraction, Oxford, UK) equipped with a CCD detector, and using graphite-monochromatized MoK α radiation ($\lambda = 0.71073 \text{ \AA}$).

All the members of the cylindrite homologous series (see Appendix A and references [16–19]) exhibit a combination of a pseudo-tetragonal (pseudo-quadratic layer, labeled Q) with a pseudo-hexagonal layer (labeled H). The Q layer is a (100) slab of the PbS/NaCl archetype, two to four atoms thick (for instance, two in cylindrite, four in franckeite); the H layer is a CdI₂-type layer that can be one-octahedron thick (as in cylindrite) or two-octahedra thick (as in cannizzarite) [19]. Although cylindrite-like synthetic compounds with H layers of the NbS₂/TaS₂-type (with cations in a triangular prismatic coordination, one, two or three layers thick, and van der Waals bonding between H layers in the multiple-layer cases) have been described ([20] and references therein), merelaniite (with MoS₂ layers) represents the first case of triangular-prismatic coordination of the H layers occurring in nature. In the following, the *a* and *b* directions are parallel to the layers, and *c* is the layer-stacking direction, and *a*_H is parallel to *b*_Q. The orientation of the *a* and *b* directions relative to the whisker axis is currently unknown.

Although the diffraction quality was very poor (Figure 10), we were able to determine the cell values for the two centered pseudo-tetragonal and pseudo-hexagonal sublattices (*H* and *Q* pseudo-layers, respectively):

Q pseudo-layer: (obtained by least-squares refinement of 41 reflections)

Triclinic	Space group: C1 or C $\bar{1}$	
$a = 5.929(8) \text{ \AA}$	$b = 5.961(5) \text{ \AA}$	$c = 12.03(1) \text{ \AA}$
$\alpha = 91.33(9)^\circ$	$\beta = 90.88(5)^\circ$	$\gamma = 91.79(4)^\circ$
$V = 425(2) \text{ \AA}^3$	$Z = 4$	

H pseudo-layer: (obtained by least-squares refinement of 29 reflections)

Triclinic	Space group: C1 or C $\bar{1}$	
$a = 5.547(9) \text{ \AA}$	$b = 3.156(4) \text{ \AA}$	$c = 11.91(1) \text{ \AA}$
$\alpha = 89.52(9)^\circ$	$\beta = 92.13(5)^\circ$	$\gamma = 90.18(4)^\circ$
$V = 208(2) \text{ \AA}^3$	$Z = 2$	

About 35 small fragments were studied with an Oxford Diffraction Excalibur PX Ultra diffractometer fitted with a 165 mm diagonal Onyx CCD detector and using copper radiation (CuK α , $\lambda = 1.54138 \text{ \AA}$) at the CRIST centre of the University of Florence, Italy. Most of the grains did not diffract as “single-crystals” and, for this reason, overexposed (from 10 to 60 h) rotation photographs were collected. The program *CrysAlis* RED was used to convert the observed diffraction rings to a conventional powder diffraction pattern (Tables 3 and 4). The X-ray diffraction pattern was indexed according to the two centered pseudo-tetragonal and pseudo-hexagonal sublattices (*H* and *Q* pseudo-layers, respectively). The least squares refinement gave the following values:

Q pseudo-layer:

Triclinic	Space group: C1 or $C\bar{1}$	
$a = 5.9249(8)$	$b = 5.987(3)$	$c = 12.077(6)$ Å
$\alpha = 90.61(3)^\circ$	$\beta = 90.04(2)^\circ$	$\gamma = 89.95(3)^\circ$
$V = 428.4(9)$ Å ³	$Z = 4$	

H pseudo-layer:

Triclinic	Space group: C1 or $C\bar{1}$	
$a = 5.5503(6)$	$b = 3.1536(8)$	$c = 11.877(1)$ Å
$\alpha = 90.00(1)^\circ$	$\beta = 90.05(1)^\circ$	$\gamma = 89.92(2)^\circ$
$V = 207.9(7)$ Å ³	$Z = 2$	

Comparisons of merelaniite's crystallographic data with other members of the cylindrite homologous series are presented in Appendix A.

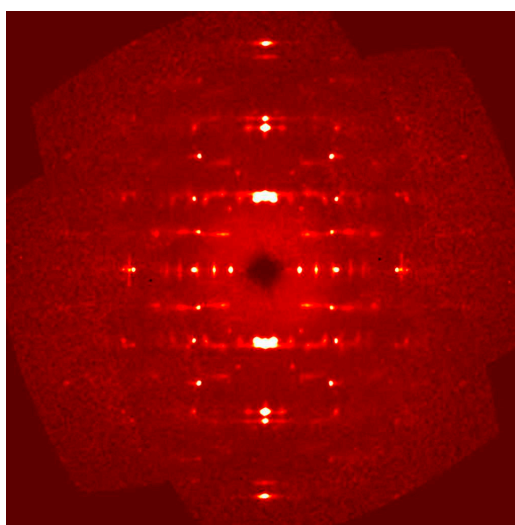


Figure 10. Reconstructed precession image of the [001] zone of a single merelaniite whisker (sample 3665LB) obtained with single-crystal X-ray diffraction.

Table 3. X-ray diffraction data (using $\text{CuK}\alpha$) belonging to the Q-subcell of merelaniite. The two most intense reflections are indicated in boldface type.

h	k	l	d (Å)	I
0	0	2	6.14	30
1	1	1	3.96	15
0	0	4	3.01	10
2	0	0	2.965	100
1	1	4	2.444	10
2	0	3	2.384	5
0	1	5	2.230	5
3	1	1	1.852	20
3	1	2	1.790	15
2	2	5	1.582	5
2	3	5	1.360	5

The X-ray diffraction study was coupled with a transmission electron microscope (TEM) investigation, which was done by means of a JEOL JEM-2010 TEM (Akishima, Tokyo, Japan) operating at 200 keV and 0.3 pA/cm² current density. Selected area electron diffraction (SAED) patterns were obtained with the intermediate lens adjusted to produce cross-over at the back focal plane. Some samples were prepared by crushing whiskers mechanically in ethanol and allowing

drops of the mixture to evaporate on a copper TEM grid. In addition, after many failed attempts, one sample was successfully prepared using a Leica Ultracut UCT ultramicrotome (Leica Microsystems, Vienna, Austria) on a whisker embedded in epoxy and cut normal to the whisker axis using a DiATOME diamond knife (DiATOME, Hatfield, PA, USA). High-resolution TEM images were obtained from crushed and ultramicrotomed samples, and SAED patterns were obtained from the ultramicrotomed sample.

Table 4. X-ray diffraction data (using $\text{CuK}\alpha$) belonging to the H -subcell of merelaniite. The three most intense reflections are indicated in boldface type.

h	k	l	d (Å)	I
0	0	2	5.94	60
1	0	2	4.05	15
0	0	4	2.968	25
1	1	1	2.673	20
2	0	3	2.272	40
3	0	1	1.829	30
3	1	0	1.596	15
3	1	2	1.542	5
2	0	7	1.448	5
3	0	6	1.350	5
1	1	8	1.305	10
3	2	0	1.201	5
2	1	9	1.115	10

In Figure 11 a selected area electron diffraction pattern of the $hk0$ layer is presented. The two centered pseudo-tetragonal and pseudo-hexagonal sublattices are clearly visible (red and yellow circles refer to the H and Q pseudo-layers, respectively). An estimation of the cell edges of the red centered cell (Q pseudo-layer) gave $a \approx 5.93$ and $b \approx 5.97$ Å, whereas the cell edges of the yellow centered cell (H pseudo-layer) are $a \approx 5.58$ and $b \approx 3.21$ Å. The electron diffraction pattern down (010) is shown in Figure 12. A value of ≈ 12 Å for the c -axis can be measured, which is in agreement with the c -axis of the $2H$ polytype of molybdenite (i.e., 12.3 Å [21]). The alternation of the two centered pseudo-layers is also clearly visible in the high-resolution TEM image shown in Figure 13, and the c -axis of about 12 Å is confirmed. The undulating curved appearance of the PbS-type and MoS₂-type modules stacked along the (001) is a typical feature of the members of the cylindrite group [22,23] (Figure 14).

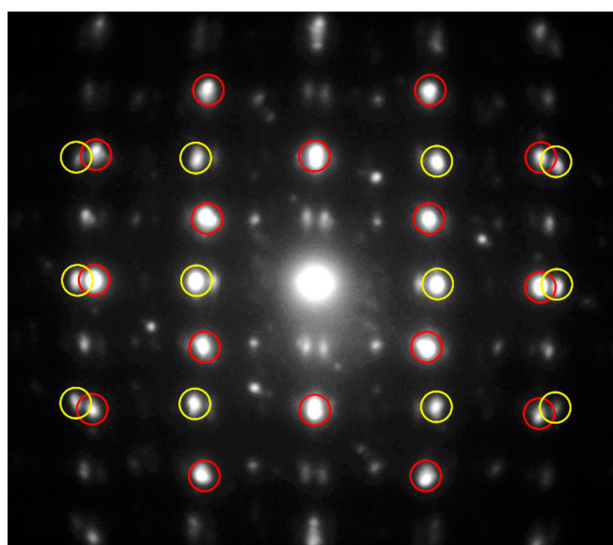


Figure 11. Selected area electron diffraction pattern down (001) of merelaniite. Red and yellow circles refer to the H and Q pseudo-layers, respectively. (Sample 3666qx A grid A2.).

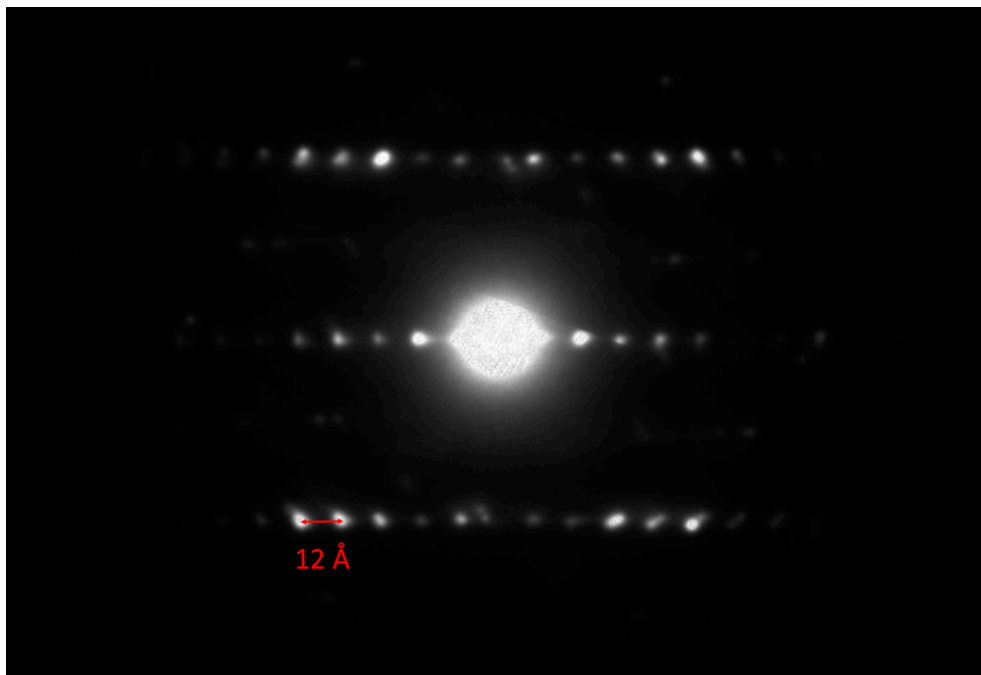


Figure 12. Selected area electron diffraction pattern down [010] of merelaniite. The *c*-stacking corresponding to ≈ 12 Å is shown. (Sample 3666qx A grid A2.).

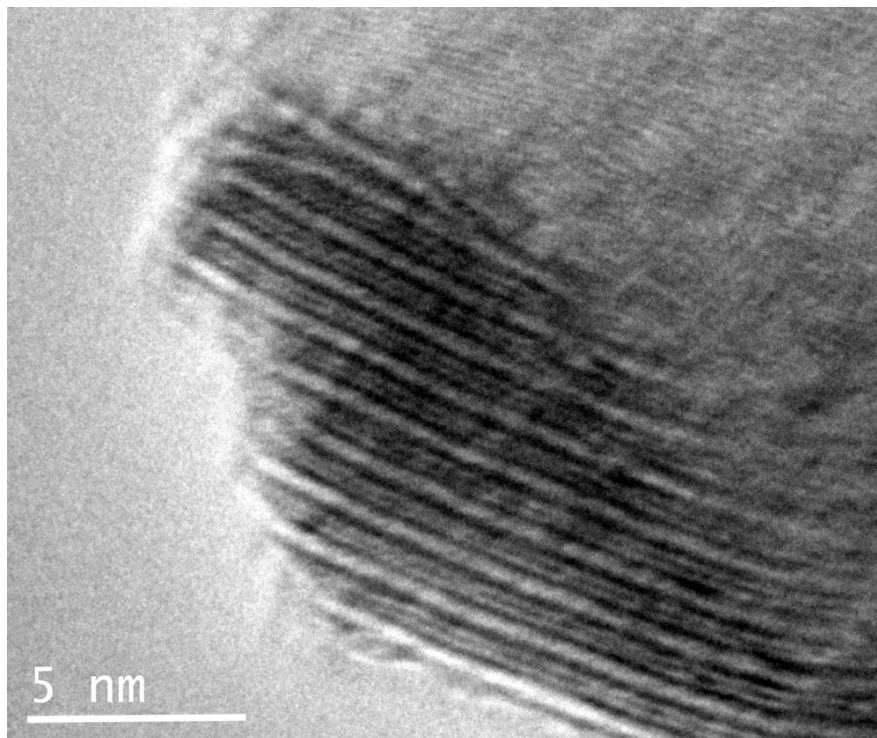


Figure 13. High-resolution TEM image showing the modulated stacking along the *c*-axis of the PbS-type (*Q*) and MoS₂-type (*H*) layers. Sample prepared by mechanical crushing of a whisker. The length of the scale bar is approximate. (Sample 3666qf.)

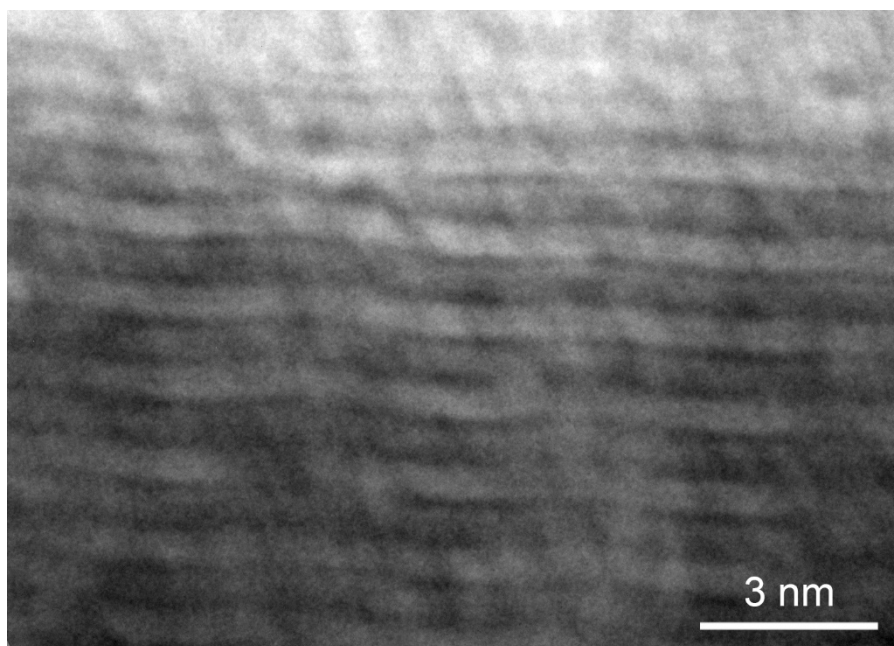


Figure 14. High-resolution transmission electron microscopy (TEM) image showing undulations in the PbS-type (*Q*) and MoS₂-type (*H*) layers, which are stacked along the *c*-axis. Sample (3666qx A grid A2) prepared by ultramicrotome. The length of the scale bar is approximate.

4. Discussion

4.1. Incommensurability of the Two Pseudo-Layers

The question of the long-distance regularity must be related to the question of semi-commensurability along the modulation direction. Along that direction, the *Q* and *H* parameters are typically in the ratio of two successive integers: for example, cylindrite exhibits the 13*Q*/12*H* match, and franckeite, depending upon the Sn²⁺ for Pb substitution, shows a match that varies from 12*Q*/11*H* for the Sn²⁺-richest member (“*incaite*”) up to 16*Q*/15*H* for the Sn²⁺-free member (“*potosiite*”).

If we calculate the ratio between *a_H* and *b_Q* (equivalent to the *c_H*/*c_Q* in reference [20]), we obtain 0.93055. This leads to a 13*Q*/14*H* ratio for merelaniite (77.58 Å with a delta = 0.165 Å), which represents the first case of *n_Q* < *n_H*. This is obviously due to the small *H* pseudo-layer in merelaniite because of the presence of Mo.

4.2. Inferred Crystal-Chemical Formula of the Two Pseudo-Layers

The calculation of the surfaces of the two layers perpendicular to the *c*-axis leads to the following: On the basis of sub-systems cell values by single-crystal X-ray diffraction:

$$S_Q = a_Q \times b_Q = 35.32 \text{ \AA}^2$$

$$S_H = a_H \times b_H = 17.51 \text{ \AA}^2.$$

On the basis of sub-systems cell values by powder X-ray diffraction:

$$S_Q = a_Q \times b_Q = 35.47 \text{ \AA}^2$$

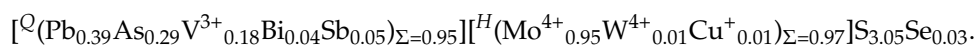
$$S_H = a_H \times b_H = 17.50 \text{ \AA}^2.$$

As the two *Q* and *H* subcells correspond to centered pseudo-tetragonal and pseudo-hexagonal lattices, and because we measured a *c*-axis of about 12 Å (see above), merelaniite should contain

$[2(M_2S_2)]$ and $[1(M'_2S_4)]$ atoms, respectively [24]. For the whole structure, considering one unit H subcell, which contains $[1(M'_2S_4)]$ atoms, for the same volume, the Q part will correspond to $([2(M_2S_2)] \times S_H/S_Q)$ atoms. As $S_H/S_Q \approx 0.50$ (0.496 and 0.493 from single-crystal and powder data, respectively), the structural formula of merelaniite can be written as: $[2(M_2S_2)]_{0.50} \cdot [(M'_2S_4)]$, which is consistent with the electron microprobe results yielding a metal to sulfur ratio ($M:S$) of 2:3. Recalculation of the formula from the electron microprobe results on the basis of two metal atoms, or, alternatively, on the basis of five atoms (two cations + three anions) and following the crystal-chemical preference of the elements usually reported in minerals and synthetic compounds belonging to the cylindrite group [24], and also assuming V and W are trivalent and tetravalent, respectively, gives



Interestingly, as mentioned in the chemistry section, we identified a bimodal composition to some of the whiskers, which might also be observed optically (Figure 6). After characterizing both compositions (from a chemical and structural point of view) it is clear there are strong As-enrichments that cause the bimodality. We thought that this could represent a different mineral than merelaniite but a recalculation of the average chemistry on the same basis described above led to the following formula:



Based on the average compositions it therefore appears prudent to conclude that Pb and Mo always dominate the respective Q and H pseudo-layers, and therefore the As -rich phases do not deserve the status of being an independent mineral; however, this remains a distinct possibility subject to further directed compositional studies.

Acknowledgments: John A. Jaszczak acknowledges Jessica Simonoff and Robert Simonoff for first noticing these unusual crystals and facilitating the initial collaboration with Michael A. Wise. We are grateful to Simon Harrison for generously sharing specimens that led to the discovery of sufficient material to make this study possible. Stephen A. Hackney and John A. Jaszczak thank Owen P. Mills (Applied Chemical and Morphological Analysis Laboratory, Michigan Technological University) for assistance with TEM work and related sample preparation. John A. Jaszczak also thanks Dan Seguin (Michigan Technological University) for assistance preparing polished sections. Mark Welch is thanked for his preliminary single-crystal X-ray diffraction studies. We are also grateful to Yoke-Khin Yap (Michigan Technological University) and André J. Sommer (Miami University, Oxford, OH, USA) for allowing the use of their Raman spectrometer systems for this study.

Author Contributions: John A. Jaszczak and Michael S. Rumsey determined assemblages, occurrences, and geological information. Chris J. Stanley, Michael S. Rumsey and John A. Jaszczak determined optical and physical properties, Michael A. Wise, Michael S. Rumsey, and John Spratt conducted electron microprobe experiments and Michael S. Rumsey performed the data analysis. John A. Jaszczak carried out SEM, EDS, and Raman spectroscopy experiments. Luca Bindi and Michael S. Rumsey conducted X-ray diffraction experiments and Luca Bindi performed the associated data analysis on the X-ray and TEM diffraction data. TEM studies were conducted by Stephen A. Hackney and John A. Jaszczak. John A. Jaszczak, Michael S. Rumsey and Luca Bindi wrote the paper.

Conflicts of Interest: The authors declare no conflict of interest.

Appendix A. Relation to Other Species

Merelaniite, $\text{Mo}_4\text{Pb}_4\text{VSbS}_{15}$, is a new member of the cylindrite homologous series (Table A1) [18,19]. The series includes the following cylindrite-type minerals (cylindrite, lévyclauidite, abramovite), and franckeite-type minerals (franckeite, “potosiite”, “incaite”, coiraitite). Merelaniite is related to cylindrite and franckeite by the isovalent substitution $2\text{Sn}^{4+} \rightarrow 2\text{Mo}^{4+}$ and the mechanism $2\text{Sn}^{2+} + \text{Fe} + 2\text{Sb} \rightarrow 2\text{Mo}^{4+} + \text{V} + \text{Sb} + \text{S}$. Merelaniite is also related to abramovite by the mechanisms: 2Bi (in abramovite) $\rightarrow \text{V}^{3+} + \text{Sb}$ (in merelaniite) and 2SnIn (in abramovite) $\rightarrow 4\text{Mo} + \text{S}$ (in merelaniite).

Table A1. Comparative data for minerals of the cylindrite homologous series [18,19]. (See references for details regarding the specific crystallographic setting conventions employed.)

Species	Formula (Approximate)	Unit Cell Parameters and Major X-ray Reflections [<i>d</i> in Å and (Relative Intensity)]	References
<i>Cylindrite type:</i>			
cylindrite	FePb ₃ Sn ₄ Sb ₂ S ₁₄	Q layer: $a = 11.733(5), b = 5.790(8), c = 5.810(5) \text{ \AA}$ $\alpha = 90.0(2)^\circ, \beta = 92.38(20)^\circ, \gamma = 93.87(20)^\circ$ H layer: $a = 11.709(5), b = 3.670(8), c = 6.320(5) \text{ \AA}$ $\alpha = 90.0(2)^\circ, \beta = 92.58(20)^\circ, \gamma = 90.85(20)^\circ$ Reflections: 5.73 (50) 4.25 (30) 3.85 (100) 3.41 (40) 2.88 (100) 2.30 (30) 2.04 (50) 1.81 (40)	[16,17,19,20,23,25]
lévyclaudite	Cu ₃ Pb ₈ Sn ₇ (Bi,Sb) ₃ S ₂₈	Q layer: $a = 11.84(1), b = 5.825(10), c = 5.831(10) \text{ \AA}$ $\alpha = 90^\circ, \beta = 92.6^\circ, \gamma = 90^\circ$ H layer: $a = 11.84(1), b = 3.67(1), c = 6.31(1) \text{ \AA}$ $\alpha = 90^\circ, \beta = 92.58^\circ, \gamma = 90^\circ$ Reflections: 5.91 (5) 4.06 (30) 3.93 (100) 3.17 (20) 2.95 (20) 2.92 (100) 2.82 (30) 2.068 (30) 2.038 (10)	[18–20]
merelaniite	Mo ₄ Pb ₄ VSbS ₁₅	Q layer: $a = 5.929(8), b = 5.961(5), c = 12.03(1) \text{ \AA}$ $\alpha = 91.33(9)^\circ, \beta = 90.88(5)^\circ, \gamma = 91.79(4)^\circ$ $V = 425(2) \text{ \AA}^3, Z = 4$ H layer: $a = 5.547(9), b = 3.156(4), c = 11.91(1) \text{ \AA}$ $\alpha = 89.52(9)^\circ, \beta = 92.13(5)^\circ, \gamma = 90.18(4)^\circ$ $V = 208(2) \text{ \AA}^3, Z = 2$ Reflections: 6.14 (30) 5.94 (60) 4.05 (15) 3.96 (15) 3.01 (10) 2.968 (25) 2.965 (100) 2.673 (20) 2.444 (10) 2.272 (40) 1.852 (20) 1.829 (30)	(this study)
abramovite	Pb ₂ SnInBiS ₇	Q layer: $a = 23.4(3), b = 5.77(2), c = 5.83(1) \text{ \AA}$ $\alpha = 89.1(5)^\circ, \beta = 89.9(7)^\circ, \gamma = 91.5(7)^\circ$ $V = 790(8) \text{ \AA}^3$ H layer: $a = 23.6(3), b = 3.6(1), c = 6.2(1) \text{ \AA}$ $\alpha = 91(2)^\circ, \beta = 92(1)^\circ, \gamma = 90(2)^\circ$ $V = 532(10) \text{ \AA}^3$ Reflections: 5.90 (36) 3.90 (100) 3.84 (71) 3.17 (26) 2.92 (33) 2.90 (16) 2.33 (15) 2.19 (18) 2.04 (20) 1.46 (6)	[26]
<i>Franckeite type:</i>			
coiraite	(Pb,Sn ²⁺) _{12.5} As ₃ Fe ²⁺ Sn ⁴⁺ ₅ S ₂₈	Q layer: $a = 5.84(1) \text{ \AA}, b = 5.86(1) \text{ \AA}, c = 17.32(1) \text{ \AA}$ $\beta = 94.14(1)^\circ$ $V = 590.05(3) \text{ \AA}^3, Z = 4$ H layer (orthogonal setting): $a = 6.28(1) \text{ \AA}, b = 3.66(1) \text{ \AA}, c = 17.33(1) \text{ \AA}$ $\beta = 91.46(1)^\circ$ $V = 398.01(6) \text{ \AA}^3, Z = 2$ Reflections: 5.78 (20) 4.34 (40) 3.46 (30) 3.339 (20) 2.876 (100) 2.068 (60)	[24]

Table A1. Cont.

Species	Formula (Approximate)	Unit Cell Parameters and Major X-ray Reflections [<i>d</i> in Å and (Relative Intensity)]	References
<i>Franckeite type:</i>			
franckeite	Fe(Pb,Sn ²⁺) ₆ Sn ⁴⁺ ₂ Sb ₂ S ₁₄ Pb _{21.74} Sn _{9.34} Fe _{3.95} Sb _{8.08} S _{56.87}	Q layer:	[23,27,28]
		<i>a</i> = 5.805(8), <i>b</i> = 5.856(16) Å, <i>c</i> = 17.338(5) Å	
		$\alpha = 94.97(2)^\circ$, $\beta = 88.45(2)^\circ$, $\gamma = 89.94(2)^\circ$	
		H layer:	
		<i>a</i> = 3.665(8), <i>b</i> = 6.2575(16), <i>c</i> = 17.419(5) Å	
		$\alpha = 95.25(2)^\circ$, $\beta = 95.45(2)^\circ$, $\gamma = 89.97(2)^\circ$	
		Reflections: 8.632 (13) 5.775 (12) 4.325 (34) 3.458 (100) 2.915 (6) 2.879 (78) 2.160 (8)	
"incaite"	FePb ₄ Sn ²⁺ ₂ Sn ⁴⁺ ₂ Sb ₂ S ₁₄		
"potosiite"	FePb ₆ Sn ⁴⁺ ₂ Sb ₂ S ₁₄		

References

- Simonoff, J.A.; Wise, M.A. A closer look at Merelani minerals. *Miner. News* **2012**, *28*, 10.
- Simonoff, J.A.; Wise, M.A. More on Merelani minerals. *Miner. News* **2012**, *28*, 3.
- Simonoff, J.; Wise, M.A. Minerals of the tanzanite-prehnite association from Merelani Hills, Tanzania. *Rocks Miner.* **2014**, *89*, 182.
- Zakrzewski, M.A.; Burke, E.A.J.; Lustenhouwer, W.J. Vuorelaincite, a new spinel, and associated minerals from the Sättra (Doverstorp) pyrite deposit, central Sweden. *Can. Miner.* **1982**, *20*, 281–290.
- Smith, D.G.W.; Nickel, E.H. A System of Codification for Unnamed Minerals: Report of the Subcommittee for Unnamed Minerals of the IMA Commission on New Minerals, Nomenclature and Classification. *Can. Miner.* **2007**, *45*, 983–1055. [CrossRef]
- Yanulova, M.K.; Kosyak, E.A. Mineral form of occurrence of molybdenum in the Kayrakty ore deposit. *Tr. Inst. Geol. Nauk Akad. Nauk Kaz. SSR* **1971**, *31*, 162–167. (In Russian)
- Harrison, S.; Jaszczak, J.A.; Keim, M.; Rumsey, M.; Wise, M.A. Spectacular Sulfides from the Merelani Tanzanite Deposit, Manyara Region, Tanzania. *Mineral. Rec.* **2014**, *45*, 553–570.
- Olivier, B. The Geology and Petrology of the Merelani Tanzanite Deposit, Tanzania. Ph.D. Thesis, Stellenbosch, South Africa, 2006. Available online: <https://scholar.sun.ac.za/bitstream/handle/10019.1/1093/olivier-b-2008.pdf?sequence=3&isAllowed=y> (accessed on 29 August 2016).
- Harris, C.; Hlongwane, W.; Gule, N.; Scheepers, R. Origin of tanzanite and associated gemstone mineralization at Merelani, Tanzania. *S. Afr. J. Geol.* **2014**, *117*, 15–30. [CrossRef]
- Weiss, S.; Jaszczak, J.A.; Harrison, S.; Hintze, J.; Radl, W. Merelani: Tansanit und seltene Sammlermineralien. *Lapis* **2015**, *40*, 34–63. (In German)
- Feneyrol, J.; Giuliani, G.; Ohnenstetter, D.; Fallick, A.E.; Martelat, J.E.; Monié, P.; Dubessy, J.; Rollion-Bard, C.; Le Goff, E.; Malisa, A.; et al. New aspects and perspectives on tsavorite deposits. *Ore Geol. Rev.* **2013**, *53*, 1–25. [CrossRef]
- Lafuente, B.; Downs, R.T.; Yang, H.; Stone, N. The power of databases: The RRUFF project. In *Highlights in Mineralogical Crystallography*; Armbruster, T., Danisi, R.M., Eds.; W. De Gruyter: Berlin, Germany, 2015; pp. 1–30.
- Zhang, X.; Qiao, X.-F.; Shi, W.; Wu, J.-B.; Jiang, D.-S.; Tan, P.-H. Phonon and Raman scattering of two-dimensional transition metal dichalcogenides from monolayer, multilayer, to bulk material. *Chem. Soc. Rev.* **2015**, *44*, 2757–2785. [CrossRef] [PubMed]
- Fan, J.-H.; Gao, P.; Zhang, A.-M.; Zhu, B.-R.; Zheng, H.-L.; Cui, X.-D.; He, R.; Zhang, Q.-M. Resonance Raman scattering in bulk 2H-MX₂ (M = Mo, W; X = W, Se) and monolayer MoS₂. *J. Appl. Phys.* **2014**, *115*, 053527. [CrossRef]
- Baranov, A.V.; Bogdanov, K.V.; Ushakova, E.V.; Cherevkov, S.A.; Fedorov, A.V.; Tscharnatke, S. Comparative analysis of Raman spectra of PbS macro- and nanocrystals. *Opt. Spectrosc.* **2010**, *109*, 268–271. [CrossRef]

16. Makovicky, E. Microstructure of cylindrite. *Neues Jahrb. Mineral. Monat.* **1971**, 404–413.
17. Makovicky, E. Mineralogical data on cylindrite and incaite. *Neues Jahrb. Mineral. Monat.* **1974**, 235–256.
18. Makovicky, E.; Hyde, B.G. Incommensurate, two-layer structures with complex crystal chemistry: Minerals and related synthetics. *Mater. Sci. Forum* **1992**, 100–101, 1–100. [[CrossRef](#)]
19. Moëlo, Y.; Makovicky, E.; Mozgova, N.N.; Jambor, J.L.; Cook, N.; Pring, A.; Paar, W.H.; Nickel, E.H.; Graeser, S.; Karup-Møller, S.; et al. Sulphosalt systematics: A review. Report of the sulphosalt sub-committee of the IMA Commission on Ore Mineralogy. *Eur. J. Miner.* **2008**, 20, 7–46.
20. Evain, M.; Petříček, V.; Moëlo, Y.; Maurel, C. First (3 + 2)-dimensional superspace approach to the structure of levyclaudite-(Sb), a member of the cylindrite-type minerals. *Acta Crystallogr.* **2006**, B62, 775–789. [[CrossRef](#)] [[PubMed](#)]
21. Schonfeld, B.; Huang, J.J.; Moss, S.C. Anisotropic mean-square displacements (MSD) in single crystals of 2H- and 3R-MoS₂. *Acta Crystallogr.* **1983**, B39, 404–407. [[CrossRef](#)]
22. Makovicky, E.; Petříček, V.; Dušek, M.; Topa, D. Crystal structure of a synthetic tin-selenium representative of the cylindrite structure type. *Am. Miner.* **2008**, 93, 1787–1798. [[CrossRef](#)]
23. Williams, T.B.; Hyde, B.G. Electron microscopy of cylindrite and franckeite. *Phys. Chem. Miner.* **1988**, 15, 521–544. [[CrossRef](#)]
24. Paar, W.H.; Moëlo, Y.; Mozgova, N.N.; Organova, N.I.; Stanley, C.J.; Roberts, A.C.; Culetto, F.J.; Effenberger, H.S.; Topa, D.; Putz, H.; et al. Coiraitite, (Pb,Sn²⁺)_{12.5}As₃Fe²⁺Sn⁴⁺₅S₂₈, a franckeite-type new mineral species from Jujuy Province, NW Argentina. *Miner. Mag.* **2008**, 72, 1083–1101. [[CrossRef](#)]
25. Makovicky, E. Crystallography of cylindrite. Part I. Crystal lattices and incaite. *Neues Jahrb. Mineral. Abh.* **1976**, 126, 304–326.
26. Yudovskaya, M.A.; Trubkin, N.V.; Koporulina, E.V.; Belakovsky, D.I.; Mokhov, A.V.; Kuznetsova, M.V.; Golovanova, T.I. Abramovite, Pb₂SnInBiS₇, a new mineral species from fumaroles of the Kudryavy volcano, Kurile Islands, Russia. *Geol. Ore Dep.* **2008**, 50, 551–555. [[CrossRef](#)]
27. Mottana, A.; Fiori, S.; Parodi, G.C. Improved X-ray powder diffraction data for franckeite. *Powder Diffr.* **1992**, 7, 112–114. [[CrossRef](#)]
28. Makovicky, E.; Petříček, V.; Dušek, M.D.; Topa, D. The crystal structure of franckeite, Pb_{21.7}Sn_{9.3}Fe_{4.0}Sb_{8.1}S_{56.9}. *Am. Miner.* **2011**, 96, 1686–1702.



© 2016 by the authors; licensee MDPI, Basel, Switzerland. This article is an open access article distributed under the terms and conditions of the Creative Commons Attribution (CC-BY) license (<http://creativecommons.org/licenses/by/4.0/>).